ISSN 1674-1056
http://cpb.iphy.ac.cn
http://iopscience.iop.org/cpb
中国物理 B
Chinese Physics
中国物理 Chinese Physics B

Thermal properties of transition-metal dichalcogenide

Xiangjun Liu(刘向军), Yong-Wei Zhang(张永伟)
Citation: Chin. Phys. B . 2018, 27(3): 034402. **doi:** 10.1088/1674-1056/27/3/034402

Journal homepage: http://cpb.iphy.ac.cn; http://iopscience.iop.org/cpb

What follows is a list of articles you may be interested in

Thermal conductivity of carbon nanotube superlattices: Comparative study with defective carbon nanotubes

Kui-Kui Zhou(周魁葵), Ning Xu(徐 宁), Guo-Feng Xie(谢国锋)
Chin. Phys. B . 2018, 27(2): 026501. **doi:** 10.1088/1674-1056/27/2/026501

Thermal transport in twisted few-layer graphene

Min-Hua Wang(王敏华), Yue-E Xie(谢月娥), Yuan-Ping Chen(陈元平)
Chin. Phys. B . 2017, 26(11): 116503. **doi:** 10.1088/1674-1056/26/11/116503

Thermal conductivity of carbon nanoring linked graphene sheets:A molecular dynamics investigation

Gang Shi(石刚), Jianwei Zhang(张鉴炜), Yonglv He(贺雍律), Su Ju(鞠苏), Dazhi Jiang(江大志)
Chin. Phys. B . 2017, 26(10): 106502. **doi:** 10.1088/1674-1056/26/10/106502

Effects of in-plane stiffness and charge transfer on thermal expansion of monolayer transition metal dichalcogenide

Wang Zhan-Yu, Zhou Yan-Li, Wang Xue-Qing, Wang Fei, Sun Qiang, Guo Zheng-Xiao, Jia Yu
Chin. Phys. B . 2015, 24(2): 026501. **doi:** 10.1088/1674-1056/24/2/026501

Near-field radiative heat transfer in mesoporous alumina

Li Jing, Feng Yan-Hui, Zhang Xin-Xin, Huang Cong-Liang, Wang Ge
Chin. Phys. B . 2015, 24(1): 014401. **doi:** 10.1088/1674-1056/24/1/014401

TOPICAL REVIEW — Thermal and thermoelectric properties of nano materials

Thermal properties of transition-metal dichalcogenide

Xiangjun Liu(刘向军)† and Yong-Wei Zhang(张永伟)

*Institute of High Performance Computing, A*STAR, Singapore* 138632, *Singapore*

(Received 30 October 2017; revised manuscript received 26 January 2018; published online 13 February 2018)

Beyond graphene, the layered transition metal dichalcogenides (TMDs) have gained considerable attention due to their unique properties. Herein, we review the lattice dynamic and thermal properties of monolayer TMDs, including their phonon dispersion, relaxation time, mean free path (MFP), and thermal conductivities. In particular, the experimental and theoretical studies reveal that the TMDs have relatively low thermal conductivities due to the short phonon group velocity and MFP, which poses a significant challenge for efficient thermal management of TMDs-based devices. Importantly, recent studies have shown that this issue could be largely addressed by connecting TMDs and other materials (such as metal electrode and graphene) with chemical bonds, and a relatively high interfacial thermal conductance (ITC) could be achieved at the covalent bonded interface. The ITC of MoS_2/Au interface with chemical edge contact is more than 10 times higher than that with physical side contact. In this article, we review recent advances in the study of TMD-related ITC. The effects of temperature, interfacial vacancy, contact orientation, and phonon modes on the edge-contacted interface are briefly discussed.

Keywords: transition metal dichalcogenide, MoS_2, thermal conductivity, interfacial thermal conductance

PACS: 44.10.+i, 65.80.–g, 63.22.–m, 73.43.–f **DOI:** 10.1088/1674-1056/27/3/034402

1. Introduction

Two-dimensional (2D) material is a rapidly expanding research area. The great success of graphene has ignited intensive interest in other 2D materials. The layered transition metal dichalcogenides (TMDs) is one of the most widely researched classes of 2D materials beyond graphene. The TMDs are normally represented with the formula MX_2, where X is a chalcogen atom (S, Se, or Te), and M is a transition metal atom from groups IV–X (such as Ti, Mo, and W), as shown in Fig. 1.[1] In unit cell of TMDs, a transition metal atom M is sandwiched between two chalcogen atoms X, as shown in Fig. 2.

TMDs have gained significant interest due to their unique optical, electronic, mechanical and thermal properties.[3] The monolayers of all the members in this family are semiconducting with bandgaps of around 1–2eV,[4] which makes them prime candidates for electronic devices. Furthermore, unlike the indirect bandgaps for bulk TMDs, the monolayer TMDs has direct bandgaps due to their ultrathin structures (quantum confinement), which induce the changes of electronic structure in monolayer TMDs. The direct bandgap indicates that they are also well suited for optoelectronics. Indeed a wide range of different TMD-based optoelectronic devices have already been successfully fabricated, such as high-performance field-effect and thin film transistors,[5] photovoltaics,[6] and photodetectors.[7] As a member of 2D TMD family, monolayer MoS_2, has a large direct bandgap of 1.8 eV. For MoS_2 transistor, through various processing techniques, such as improving sample quality, removing absorbates, or depositing atop a high-dielectric layer, its room temperature carrier mobility can be significantly enhanced,[8–11] and close to its theoretically predicted phonon-limited intrinsic value (about 200 $cm^2 \cdot V^{-1} \cdot s^{-1}$).[12,13] Very recently, the growth of MoS_2 on insulating substrates was also realized, which enables atomically thin high-performance optoelectronic and electronic devices can be fabricated without film transfer.[14]

Thermal management is an important issue for the design and application of electronic devices, which even is becoming a limiting factor currently to the device development.[15–29] Owing to the atomic thickness of monolayer TMDs, thermal management is more challenging in TMDs-based electronics. On one hand, highly localized Joule heating in their ultrathin confined space can easily create "hot spots".[30,31] On the other hand, previous experimental[32–34] and theoretical studies[2,35–40] revealed that the thermal conductivities of monolayer TMDs are 2–3 orders lower than that of graphene. These two limitations cause a crucial bottleneck for efficient thermal management of TMD-based devices. Furthermore, similar to electron scattering at an interface, phonon scattering at an interface also plays a critical role in the nanoscale devices, which is even more crucial than the material itself.[41–43] Thus, low thermal conductivity in monolayer TMDs and thermal conductance at the interface will significantly affect performance and reliability of the TMDs-based devices.

In this article, we review the recent advances in the study of the dynamic and thermal properties of 2D TMDs from both experimental and theoretical points of view. The rest of this ar-

†Corresponding author. E-mail: liux@ihpc.a-star.edu.sg

© 2018 Chinese Physical Society and IOP Publishing Ltd

ticle is organized as follows: Section 2 introduces the phonon dispersion of TMDs, Section 3 discusses phonon relaxation time and mean free path of TMDs, Section 4 and 5 are devoted to the discussion of thermal conductivity and interfacial thermal conductance of TMDs, respectively. In Section 5, we present a brief conclusion.

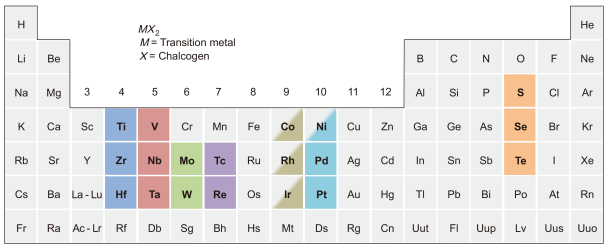


Fig. 1. (color online) Transition metals and the three chalcogen elements in the TMD layered structures. Reprinted with permission from Ref. [1], copyright (2013) by Macmillan Publishers Limited.

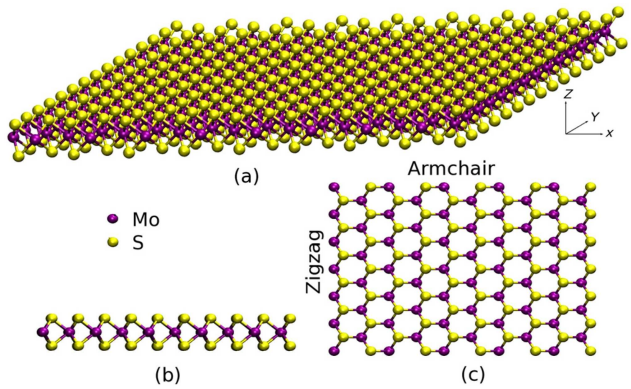


Fig. 2. (color online) (a) Structure of monolayer MoS_2. Side view (b) and top view (c) of monolayer MoS_2. The horizontal orientation is armchair direction, the vertical orientation is zigzag direction. The atoms in purple and yellow color are Mo and S, respectively. Reprinted with permission from Ref. [2], copyright (2013) by the Frontiers of Physics.

2. Phonon dispersion of TMDs

Since phonon energy is essentially the energy of atomic vibrations, to understand the thermal properties of TMDs, it is necessary to firstly inspect the lattice vibrational modes (phonons) of the materials. MoS_2 is a typical layered dichalcogenide, and the most studied material in this family. Each MoS_2 unit cell contains 3 (1 Mo and 2 S) atoms, which leads to the formation of 3 acoustic (A) and 6 optical (O) phonon modes as shown in Fig. 3(a).[44] The three acoustic phonon modes are longitudinal acoustic (LA) mode, transverse acoustic (TA) mode, and flexural acoustic (ZA) mode. LA mode corresponds to compressional waves, in which atomic displacements are along the wave propagation direction; TA mode corresponds to shear waves, in which in-plane displacements are perpendicular to the propagation direction, and ZA mode corresponds to out-of-plane atomic displacements. The phonon dispersion is the relationship between the phonon wave vector $\boldsymbol{q}$ and phonon energy E or frequency ω ($E = \hbar\omega$, where $\hbar$ is the reduced Planck constant).

The phonon dispersion and density of states (DOS) of $MoSe_2$ and WS_2 are also shown in the Figs. 3(b) and 3(c). The low-frequency acoustic phonon branches of MoS_2 up to 233 cm^{-1} are mainly from Mo(xy), S(xy), and Mo(z) vibrations due to similar mass between Mo and 2S, whereas those of WS_2 up to 182.3 cm^{-1} are mainly from the W(xy) and W(z) vibrations due to the much larger mass of W atoms.[44] These results are similar to the diatomic linear chain model, that the scale of the acoustic phonon branch/vibration is dominated by atoms with larger mass; however, the optical phonon branch/vibration is dominated by the atoms with smaller mass.[44]

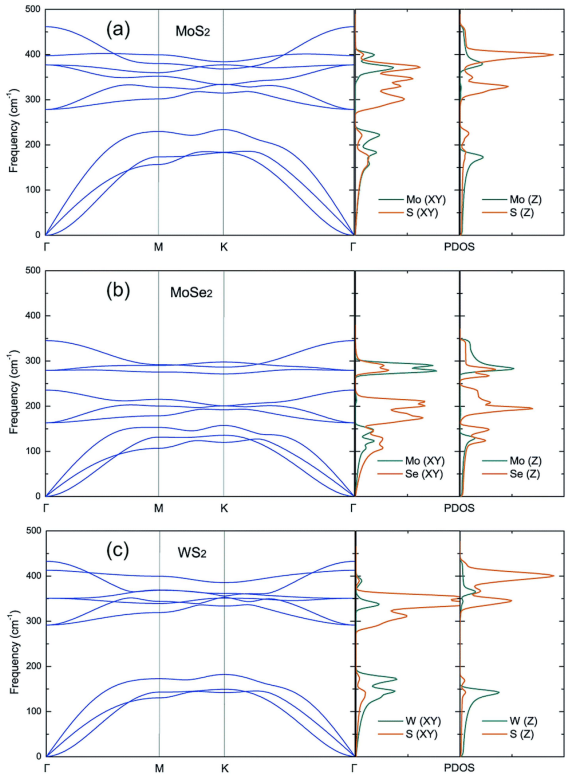


Fig. 3. (color online) Phonon dispersion and projected PDOS for (a) MoS_2, (b) $MoSe_2$, and (c) WS_2. Reprinted with permission from Ref. [44], copyright (2016) by the Royal Society of Chemistry.

At the low wave vector $\boldsymbol{q}$ near the center of Brillouin zone, the frequency of the LA and TA modes have linear dispersions[45,46] as $\omega_{\mathrm{LA}} \approx v_{\mathrm{LA}} q$ and $\omega_{\mathrm{TA}} \approx v_{\mathrm{TA}} q$, respectively. The group velocity $v_{\mathrm{LA}} \approx 1108.8$ m/s and $v_{\mathrm{TA}} \approx 693.5$ m/s are about five times lower than those (5953 m/s for LA, and 3743 m/s for TA) in graphene.[36] However, the ZA modes have an approximately quadratic dispersion,[45–47] The phonon group velocity $v = \mathrm{d}\omega/\mathrm{d}q$ with relationships of $\boldsymbol{q}$ and ω along the Γ–M high symmetrical line are shown in Fig. 4. For the LA and TA modes, the group velocities dramatically decrease with the increase of phonon frequency; while for the ZA mode, its group velocity increases with increasing frequency, and reaches the maximum value at the middle point of the Γ–M line, then decreases to zero at the zone edge.[36]

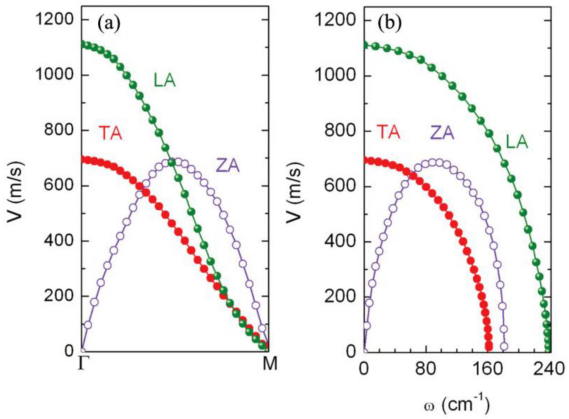


Fig. 4. (color online) Phonon group velocity of acoustic phonon modes along the Γ–M direction in MoS_2 with a function of wave number (a) and frequency (b). Reprinted with permission from Ref. [36], copyright (2014) by American Physical Society.

3. Phonon relaxation time and mean free path

Phonons have relaxation times as they travel through the materials due to various scattering processes, such as phonon–phonon umklapp scattering, boundary scattering, and defects scattering. Since extrinsic boundary scattering and defects scatting can be removed by improving material quality, the phonon–phonon umklapp scattering is highly associated with the intrinsic phonon relaxation process/time, which can be derived through Klemens's time-dependent perturbation theory[48,49]

$$\frac{1}{\tau_{qs}} = 2\gamma_{qs}^2 \frac{k_B T}{M v^2} \frac{\omega_{qs}^2}{\omega_m}, \tag{1}$$

where τ_{qs} is the lifetime for different phonon branches, M is the atomic mass, and ω_m is the Debye frequency, T is the temperature, k_B is the Boltzmann constant, and v is the averaged sound velocity given by the relation $2/v^2 = 1/v_{LA}^2 + 1/v_{TA}^2$ around the zone center. The frequency dependence of relaxation time of LA, TA, and ZA phonons in monolayer MoS_2 sheet is shown in Fig. 5(a). The relaxation time of acoustic phonon decreases sharply as the frequency of phonon increases. The values of LA, TA, and ZA modes are 6.93, 22.17, and 48.21 ps, respectively.[36] The ZA mode has the shortest relaxation time, which is consistent with the largest Grüneissen parameter, and indicates the strongest phonon scattering. scattering.

Phonon mean free path (MFP) is a key quantity for understanding the size-dependent thermal properties. The umklapp scattering limited MFP λ can be obtained, based on the mode relaxation time τ and group velocity v. The phonon MFP for the mode at the q point with s polarization is defined as $\lambda_{qs} = v_{qs}\tau_{qs}$. Figure 5(b) shows the phonon MoS_2 as a function of frequency and phonon mode. The MFP decreases obviously with the increase of frequency. In the entire frequency regime, LA mode has the longest MFP among the LA, TA, and ZA modes, due to the combined effects of the frequency-dependent relaxation time and group velocities. The largest dominated MFP among the zone-center acoustic modes is LA mode with a value of around 18.1 nm, which is much large than that of TA mode, around 5.0 nm, which is consistent with the value of 5.2 nm by the molecular dynamics (MD) calculations.[2,36]

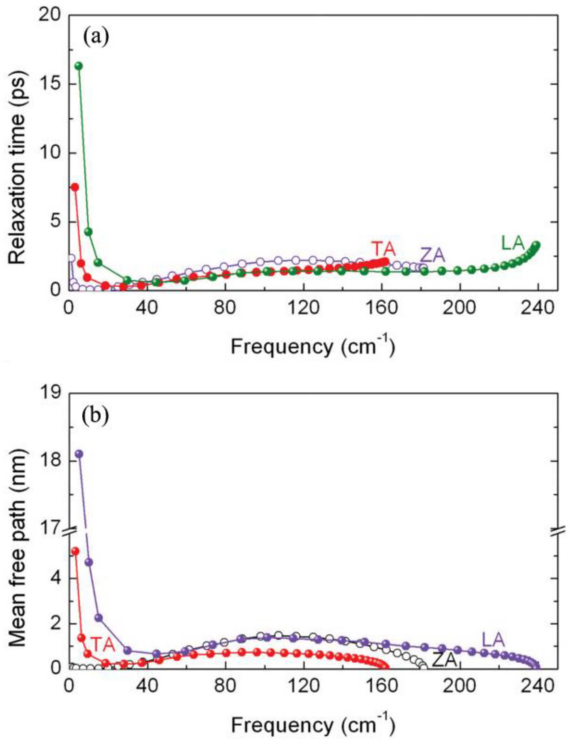


Fig. 5. (color online) (a) Relaxation time and (b) mean free path for LA, TA, and ZA modes in monolayer MoS_2 with a function of frequency. Reprinted with permission from Ref. [36], copyright (2014) by American Physical Society.

4. Thermal conductivity of monolayer TMDs

The thermal conductivity κ of monolayer TMDs can be obtained based on Fourier's law, $\kappa = -J/\nabla T$, where J is the heat flux per unit area and $\nabla T (\nabla T = dT/dz)$ is the temperature gradient along the heat flux direction. The thermal conductivity can also be related to the specific heat by $\kappa \approx \sum C v \lambda$, where C is specific heat, v and λ are the average phonon group velocity and MFP, respectively.[50] This expression is commonly used under diffusive transport conditions, where material sizes are much larger than the phonon MFP ($L \gg \lambda$).[47] During the calculation of heat flux, normally the thickness of 2D materials h is chosen to be the inter-layer spacing in the corresponding bulk materials (e.g., $h = 4.41$ Å for MoS_2[12]).

The low thermal conductivities of TMDs have been reported in both theoretical[2,36,44] and experimental[32–34,51] studies. Table 1 summarizes the reported thermal conductivities of monolayer TMDs along with their methodologies of measurement. At room temperature, the superior theoretical thermal conductivity of monolayer MoS_2

is about 103 $W \cdot m^{-1} \cdot K^{-1}$ obtained by calculating Boltzmann transport equation (BTE).[52] Its thermal conductivity is about 23.3 $W \cdot m^{-1} \cdot K^{-1}$, obtained by solving the non-equilibrium Green's function (NEGF).[37] Its experimental result is 34.5 $W \cdot m^{-1} \cdot K^{-1}$.[33] It can be found that there is a large variation between the results, which is mainly attributed to different approaches applied during the measurement. Each approach has its own advantages and disadvantages. For experimental approaches, the thermal conductivity of sample is sensitive to the defects or the substrates, which introduce extra phonon scattering and decrease the intrinsic thermal conductivity. In NEGF approach, only the harmonic force constants have been used to consider ballistic or semi-ballistic phonon transport, which ignores the anharmonic phonon–phonon scatting in the TMDs. BTE method is limited to first-order anharmonicity during the calculation. Molecular dynamics (MD) simulation is also widely used for the calculation of thermal conductivity, which naturally accounts for the lattice anharmonicity to all orders. However, the accuracy of MD simulation is limited by the quality of empirical interatomic potentials. For monolayer WSe_2, the thermal conductivity, about 3.935 $W \cdot m^{-1} \cdot K^{-1}$,[53] is one order of magnitude lower than that of MoS_2, which is due to the ultralow Debye frequency and heavy atoms mass in WSe_2. Similar to graphene, it has been found that the thermal conductivity of TMDs is also temperature dependent, which decreases with the increasing temperature.[53,54]

It has been well known that the in-plane thermal conductivity of graphene decreases significantly when it is in contact with a substrate.[47] Similar trends has also been reported for monolayer TMDs due to damping of the flexural acoustic phonon.[55] Using optothermal Raman technique, the measured thermal conductivities of suspended monolayer MoS_2 and $MoSe_2$ are 84 and 59 $W \cdot m^{-1} \cdot K^{-1}$, respectively, at room temperature. However, when they are supported on SiO_2 substrate, their thermal conductivities decrease to 55 and 24 $W \cdot m^{-1} \cdot K^{-1}$, respectively.[55]

Table 1. Summary of the thermal conductivities of different monolayer TMDs at room temperature.

TMDs	Methodologies	Type	κ ($W \cdot m^{-1} \cdot K^{-1}$)	Ref.
MoS_2	exfoliated	suspended	34.5	[33]
MoS_2	first principles calculation	suspended	23.2	[36]
MoS_2	optothermal Raman technique	suspended	84	[55]
MoS_2	Boltzmann transport equation	supported	103	[52]
MoS_2	optothermal Raman technique	supported on gold	55	[55]
WS_2	Boltzmann transport equation	suspended	142	[52]
WS_2	Raman spectroscopy	suspended	32	56
WS_2	first principles calculation	suspended	31.8	[44]
$MoSe_2$	Boltzmann transport equation	suspended	54	[52]
$MoSe_2$	first principles calculation	suspended	17.6	[44]
$MoSe_2$	optothermal Raman technique	suspended	59	[55]
$MoSe_2$	optothermal Raman technique	supported on SiO_2	24	[55]
WSe2	Boltzmann transport equation	suspended	3.935	[53]

5. Interfacial thermal conductance

Monolayer TMDs is promising in electronic and photonic device applications, such as transistors, light-emitters, and photodetectors.[57] With the successful growth of MoS_2 on insulating substrates,[14] and the significant improvement in the mobility,[58–60] it is reasonably expected that high-performance field-effect transistors based on monolayer MoS_2 will be realized in the near future. Unlike the single transistor, owing to the atomic thickness of 2D materials, thermal management of their integrated devices is becoming vitally important. The Joule heating in the confined ultrathin 2D TMDs can easily create localized hot spots. Unfortunately, previous studies[2,32–35] revealed that the monolayer TMDs have remarkable low thermal conductivity. Furthermore, phonon scattering at an interface also plays a critical role, which hinders the heat transport across the interface.[41–43,61–63] combination of these limitations poses a significant challenge for efficient thermal management of TMDs-based devices, and interfacial thermal conductance (ITC) between TMDs and other (electrode) materials will adversely affect device reliability and performance.

In general, there are two types of interface geometry between TMD sheets and other material surface: side contact and edge contact.[57]

5.1. Side contact by van der Waals interaction

Side contact can be made by contacting the basal plane of TMD sheet with other materials surface. However, the pristine surface of TMD sheet does not tend to form covalent bonds with the other material surface, and the interface across them can only interact via van der Waals forces, thus normally a low ITC is expected at the side contact interface. The ITC for MoS_2/graphene interface is 13.8 $MW \cdot m^{-2} \cdot K^{-1}$, which is much lower than that for MoS_2/MoS_2 interface (44.48 $MW \cdot m^{-2} \cdot K^{-1}$in multilayer MoS_2 bulk) and for

graphene/graphene interface (212.65 MW·m^{-2}·K^{-1} in multilayer graphene bulk, graphite).[64] This lower ITC is attributed to the fact that MoS_2 and graphene have different phonon dispersion, which causes the extra interfacial phonon scattering at the MoS_2/graphene interface. The ITC for the MoS_2/SiO_2 interface is 1.7 MW·m^{-2}·K^{-1},[65] which is significantly lower than that of the MoS_2/Au interface (17.2 MW·m^{-2}·K^{-1})[66] and graphene/SiO_2 interface (87.5 MW·m^{-2}·K^{-1}).[67] The ITC across the MoS_2/*h*-BN interface is 17.0 MW·m^{-2}·K^{-1}, which is about 3 times lower than that (52.2 MW·m^{-2}·K^{-1}) of graphene/*h*-BN interface.[68]

Table 2. Summary of the interfacial thermal conductances between different monolayer MoS_2 and other materials at room temperature.

TMDs	Contacting materials	Contact type	Methodology	ITC/MW·m^{-2}·K^{-1}	Ref.
MoS_2	Si	side	experimental	0.974	69
MoS_2	SiO_2	side	experimental	1.7	65
MoS_2	gold Au	side	theoretical	17.2	66
MoS_2	gold Au	edge	theoretical	221	61
MoS_2	*h*-BN	side	experimental	17.0	68
MoS_2	graphene	side	theoretical	13.8	64
MoS_2	graphene	edge	theoretical	6420	63

5.2. Edge contact by covalent bonds

As discussed before, monolayer TMDs have very low in-plane thermal conductivities and interfacial thermal conductance at the side-contacted interface, which hinder the heat dissipation from TMDs-based integrated devices. A probable solution is to construct an edge-contacted interface with covalent bonds by fully utilizing the contacted relative high thermal conducting materials to speed up the heat dissipation of "hot-spot" in TMDs-based devices.

As a typical example, MoS_2 field effect transistor (FET), it has been reported that there exists a large contact resistance at the interface between the MoS_2 sheet and metal electrode with the side contact due to the van der Waals gap, which drastically restrains the drain current.[57] However, for the edge contact, strong overlapping of electronic orbitals exists between the MoS_2 and metal electrode, which leads to a remarkable reduction in tunnel barrier and a significant increase in electrical current. The ITC has been significantly increased from 17.2 MW·m^{-2}·K^{-1} (with side contact) to 221 MW·m^{-2}·K^{-1} (with edge contact).[61,66] So far both previous experimental[70] and theoretical[71] studies have also confirmed that the edge contact may play a key role in the efficient injection of electrons from metal to TMDs.

Although the thermal conductivity of monolayer MoS_2 is 2–3 orders lower than that of graphene, it is interesting to find that the covalent bonds formed at the MoS_2/metal interface enables its ITC to be comparable with that of graphene-metal interface. As shown in Fig. 6, different Au surfaces form different bonding configurations, causing large ITC variations, which is due to the different coordination numbers and structural symmetries at the interface. For such edge-contacted MoS_2/metal interface, it is reported that at room temperature, the ITC is primarily dominated by phonon transport, and the effect of electron-phonon coupling is negligible.[61]

Furthermore, the ITC is found temperature-dependent. Figure 7 shows the results of the temperature-dependent ITC of MoS_2/Au interface. It is seen that the ITC and heat flux across the interface increases linearly with increasing temperature. However, the interfacial temperature jump is nearly

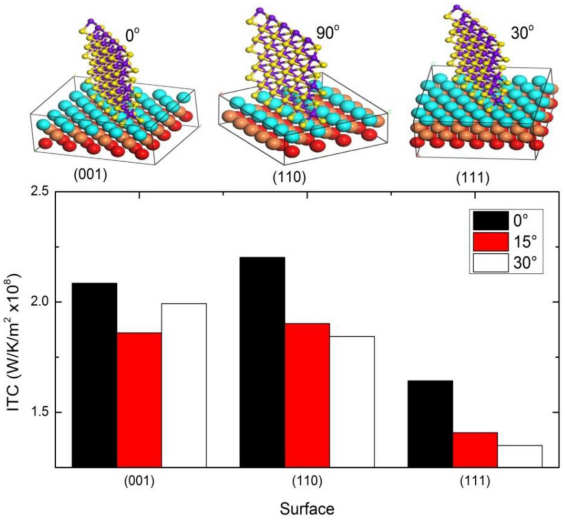


Fig. 6. (color online) Dependence of interfacial thermal conductance on Au crystal surfaces and contact directions. Reprinted with permission from Ref. [61], copyright (2016) by the Springer.

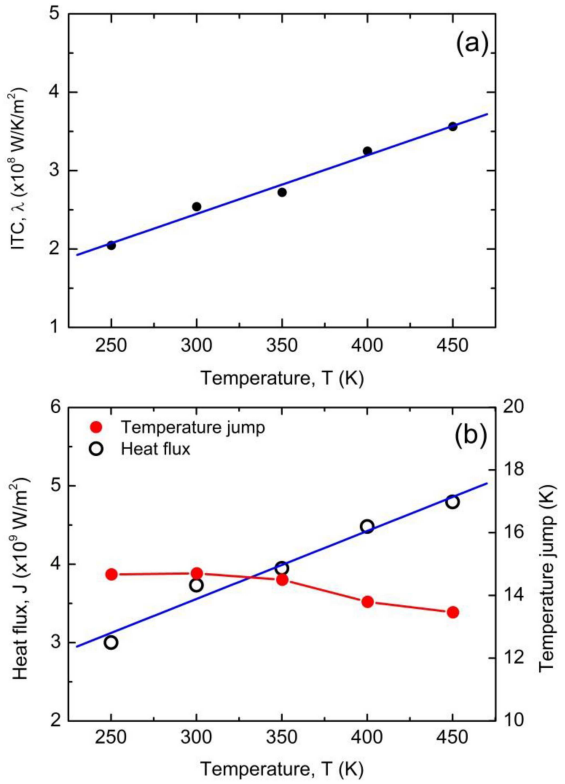


Fig. 7. (color online) (a) Interfacial thermal conductance of MoS_2/Au interface as a function of temperature; (b) interfacial temperature jump and heat flux as a function of temperature. Reprinted with permission from Ref. [61], copyright (2016) by the Springer.

independent of temperature. The trend of temperature dependence of ITC is possibly caused by the factor that, when the temperature is increased, more high-frequency phonons are excited, which contribute additional energy carriers for interfacial heat transport. Furthermore, the increasing temperature will increase the anharmonicity of atomic interactions at the interface. Eventually, the phonon transmission is enhanced through the inelastic phonon scattering. It is noted that a similar trend for such temperature-dependence was also observed in other interfaces.[72]

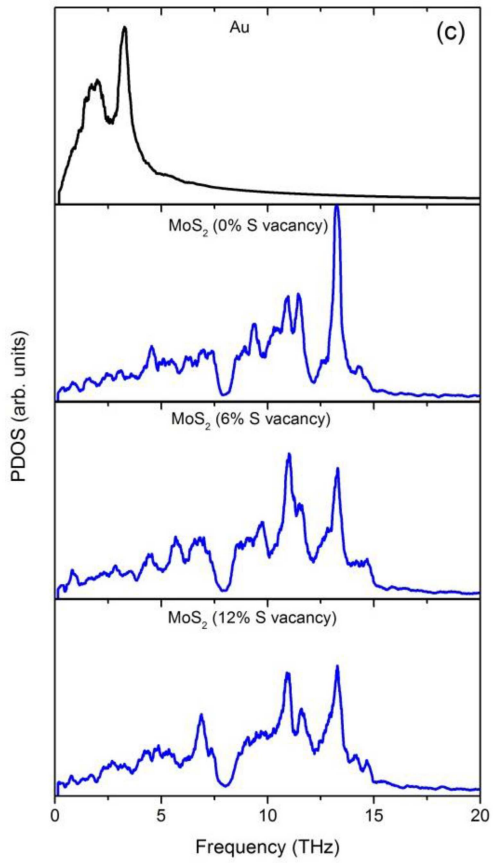


Fig. 8. (color online) Phonon density of states of Au and MoS_2 with different S vacancy concentration in the central region of MoS_2. Reprinted with permission from Ref. [61], copyright (2016) by the Springer.

Since phonon energy is essentially the energy of atomic vibrations, the analyses of energy transfer across interfaces can also be carried out in the frequency domain. From lattice dynamic point of view, the key factor that determines the phonon transport across two connecting materials is the overlapping of phonon PDOS between them.[62,63,73–75] The overlapping/similarity of PDOS two connecting materials can be quantitatively analyzed using cosine similarity measure[74]

$$S = \frac{\int D(\omega) D_0(\omega) \mathrm{d}\omega}{\left(\int D(\omega)^2 \mathrm{d}\omega\right)^{1/2} \left(\int D_0(\omega)^2 \mathrm{d}\omega\right)^{1/2}}, \qquad (2)$$

where S is the value of similarity, $D(\omega)$ and $D_0(\omega)$ are the PDOSs of two connecting materials. For the MoS_2/Au interface, the PDOS of MoS_2 has notable phonon spectrum peaks in the range larger than 8 THz with a cut-off frequency of 15 THz, as shown in Fig. 8. However, for the Au atoms, the cut-off frequency is around 5 THz, and the peaks of its PDOS are in the range lower than 5 THz. Due to the different cut-off frequency between Au and MoS_2, there is an obvious mismatch in PDOS above 5 THz at the MoS_2/Au interface, which hinders the thermal transport across the interface and causes the interfacial thermal resistance.[63]

Besides MoS_2/metal edge contact, edge contact between TMDs and other 2D materials is also an interesting and important issue. For example, unlike low thermal conducting MoS_2, another 2D counterpart, graphene, has ultra-high thermal conductivity.[76–79] Naturally, it is expected to construct edge-contacted MoS_2/graphene interface to speed up the heat transport. Figure 9 displays the schematic of MoS_2/graphene heterostructure with covalent-bonded interface. The ITC for this edge-contacted interface reaches 6420 $MW{\cdot}m^{-2}{\cdot}K^{-1}$, which is two orders higher than that of side-contacted MoS_2/graphene interface (13.8 $MW{\cdot}m^{-2}{\cdot}K^{-1}$).[63,64] Thus this edge-contacting heterostructure will be one opportunity to overcome the bottleneck in thermal management of TMDs integrated devices.

According to the molecular dynamics simulation, it is found that each covalent bond at the interface serves as an independent channel for thermal conduction, which enables the ITC to be tuned linearly by adjusting the interfacial bond density.

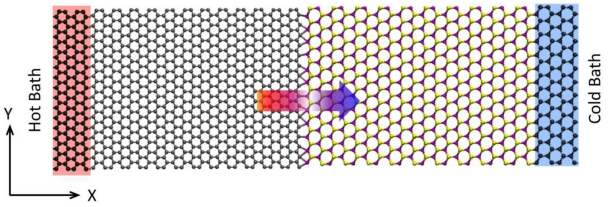


Fig. 9. (color online) In-plane MoS_2/graphene covalent-bonded heterostructure with hot and cold baths at the ends. Reprinted with permission from Ref. [63], copyright (2017) by the Springer.

The efficiency of different phonon modes transferring across the interface can be quantified by energy transmission coefficient α using the phonon wave packet method.[81,82] The energy transmission coefficient α can be obtained by $\alpha = (A_{\mathrm{tr}}/A)^2$, where A_{tr} and A are the amplitudes of transmitted and initial phonon waves at the interface, respectively. Figure 10 shows the snapshots of a wave packet near the MoS_2/graphene interface. Figure 11 shows the energy transmission coefficient of phonon wave packets. It is found that the interface effectively blocks high frequency phonon modes due to the lack of LA and TA energy states in MoS_2 at the same frequencies as in graphene. For LA phonon mode, when the incident frequencies are lower than 7.3 THz, phonon transmission coefficient α keeps around 0.75, without remarkable

change; however, it dramatically decreases, when the frequency reaches 8 THz. When the frequency is higher than 9 THz, the phonon wave packets are totally reflected.[63] In contrast to LA phonon mode, the α of TA phonons is noticeably lower than that of LA phonons, even in the low frequency regime. With the same wave vector $k_0 = 0.04\pi/a$, for LA phonon wave packet, the α is about 0.75; while for TA phonon wave packet, α is only about 0.12.[63] These results indicate that LA modes have the dominant contribution to the thermal transport across the interface.

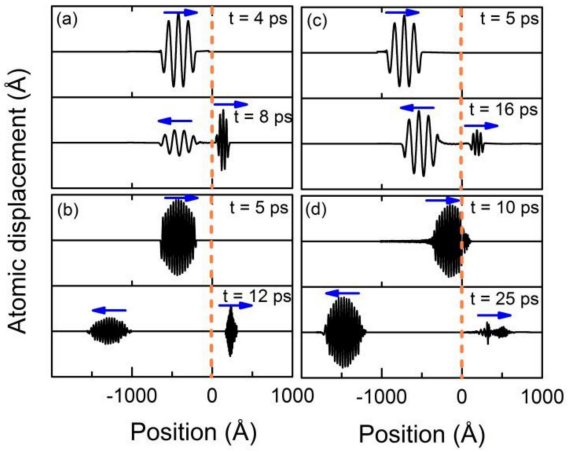


Fig. 10. (color online) Snapshots of a phonon wave packet travelling across the MoS_2/graphene interface. The travelling direction is indicated by blue arrows, and brown dashed lines denote the interface. (a) LA, $k_0 = 0.02\times2\pi/a$, $f = 1.90$ THz. (b) LA, $k_0 = 0.075\times2\pi/a$, $f = 7.10$ THz. (c) TA, $k_0 = 0.02\times2\pi/a$, $f = 1.18$ THz. (d) LA, $k_0 = 0.075\times2\pi/a$, $f = 4.41$ THz. Reprinted with permission from Ref. [63], copyright (2017) by the Springer.

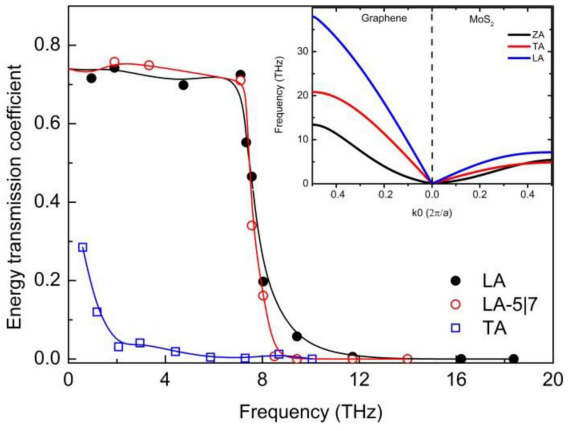


Fig. 11. (color online) Energy transmission coefficient α of a phonon wave packet as a function of frequency. The inset displays the phonon dispersion of graphene and MoS_2. The MoS_2 phonon dispersion is adopted from Ref. [36] by first principle calculations. Reprinted with permission from Ref. [63], copyright (2017) by the Springer.

Meanwhile, the rapid development in materials synthesis techniques has made many novel edge-contacted in-plane 2D heterostructures possible. For example, recently, 2D graphene/*h*-BN in-plane heterostructures were successfully synthesized.[82] In particular, it is now possible to grow atomically sharp interfaces between graphene and *h*-BN domains using combined atmospheric pressure chemical vapor deposition (CVD) and reactive ion etching.[83] These fascinating advances in the synthesis of 2D heterostructures have laid a promising foundation for realizing such edge-contacted interfaces.

6. Summary

This article presents an overview of the thermal properties of TMDs in both experimental and theoretical perspectives. The lattice dynamics and thermodynamic properties of TMDs have been summarized. The experimental and theoretical studies reveal that the TMDs have relatively low thermal conductivities, which are 2–3 orders lower than that of graphene. The low thermal conductivities pose a significant challenge for efficient thermal management of TMDs-based devices. In the context of TMDs-based electro devices, heat dissipation from the devices and interconnects is primarily limited by their low thermal conductivities and the relatively weak van der Waals interfaces. The recent studies have suggested that this issue could be largely addressed by connecting TMDs and other materials with covalent bonds, and the interfacial thermal conductance of the covalent bonded interface could be highly tunable.

Acknowledgements

We gratefully acknowledge the financial support from the Agency for Science, Technology and Research (A*STAR), Singapore and the use of computing resources at the A*STAR Computational Resource Centre, Singapore. This work is supported in part by a grant from the Science and Engineering Research Council (152-70-00017).

References

[1] Chhowalla M, Shin H S, Eda G, Li L J, Loh K P and Zhang H 2013 *Nat. Chem.* **5** 263
[2] Liu X, Zhang G, Pei Q X and Zhang Y W 2013 *Appl. Phys. Lett.* **103** 133113
[3] Fiori G, Bonaccorso F, Iannaccone G, Palacios T, Neumaier D, Seabaugh A, Banerjee S K and Colombo L 2014 *Nat. Nanotechnol.* **9** 768
[4] Kang M, Kim B, Ryu S H, Jung S W, Kim J, Moreschini L, Jozwiak C, Rotenberg E, Bostwick A and Kim K S 2017 *Nano Lett.* **17** 1610
[5] Radisavljevic B and Kis A 2013 *Nat. Mater.* **12** 815
[6] Bernardi M, Palummo M and Grossman J C 2013 *Nano Lett.* **13** 3664
[7] Lopez-Sanchez O, Lembke D, Kayci M, Radenovic A and Kis A 2013 *Nat. Nanotechnol.* **8** 497
[8] Yu Z, Pan Y, Shen Y, Wang Z, Ong Z-Y, Xu Tm Xin R, Pan L, Wang B, Sun L, Wang J, Zhang G, Zhang Y W, Shi Y and Wang X 2014 *Nat. Commun.* **5** 5290
[9] Cheng R, Jiang S, Chen Y, Liu Y, Weiss N, Cheng H C, Wu H, Huang Y and Duan X 2014 *Nat. Commun.* **5** 5143
[10] Najmaei S, Liu Z, Zhou W, Zou X, Shi G, Lei S, Yakobson B I, Idrobo J C, Ajayan P M and Lou J 2013 *Nat. Mater.* **12** 754
[11] Qiu H, Pan L, Yao Z, Li J, Shi Y and Wang X 2012 *Appl. Phys. Lett.* **100** 123104
[12] Kaasbjert K, Thygesen K S and Jacobsen W 2012 *Phys. Rev. B* **85** 115317
[13] Cai Y, Zhang G and Zhang Y W 2014 *J. Am. Chem. Soc.* **136** 6269
[14] Kang K, Xie S, Huang L, Han Y, Huang P Y, Mak K F, Kim C J, Muller D and Park J 2015 *Nature* **520** 656

[15] Zhang L M, Jiao B B, Yun S C, Kong Y M, Ku C W and Chen D P 2017 *Chin. Phys. Lett.* **34** 025101
[16] Chi F and Sun L L 2016 *Chin, Phys. Lett.* **33** 117201
[17] Jin Q X, Liu B, Liu Y, Wang W W, Wang H, Xu Z, Gao D, Wang Q, Xia Y Y, Song Z T and Feng S L 2016 *Chin. Phys. Lett.* **33** 098502
[18] Ezheiyan M, Sadeghi H and Tavakoli M H 2016 *Chin. Phys. Lett.* **33** 058102
[19] Hu R, Hu J Y, Wu R K, Xie B, Yu X J and Luo X B 2016 *Chin. Phys. Lett.* **33** 044401
[20] Nie T and Liu W Q 2012 *Acta Phys. Sin.* **61** 184401 (in Chinese)
[21] Xiao B Q, Fan J T, Jiang G P and Chen L X 2012 *Acta Phys. Sin.* **61** 154401 (in Chinese)
[22] Zhu L D, Sun F Y, Zhu J and Tang D W 2012 *Acta Phys. Sin.* **61** 134402 (in Chinese)
[23] Zhao X, Zhang W R, Jin D Y, Fu Q, Chen L, Xie H Y and Zhang Y J 2012 *Acta Phys. Sin.* **61** 134401 (in Chinese)
[24] Sun J and Liu W Q 2012 *Acta Phys. Sin.* **61** 124401 (in Chinese)
[25] Zhang G and Zhang Y W 2017 *Chin. Phys. B* **26** 034401
[26] Fu Q, Zhang W R, Jin D Y, Zhao Y X and Wang X 2016 *Chin. Phys. B* **25** 124401
[27] Hou Y and Zhu L L 2016 *Chin. Phys. B* **25** 086502
[28] Lei J M and Peng X Y 2016 *Chin. Phys. B* **25** 020202
[29] Zhang Y, Xie Z X, Deng Y X, Yu X and Li K M 2015 *Chin. Phys. B* **24** 126302
[30] Balandin A A 2011 *Nat. Mater.* **10** 569
[31] Pop E 2010 *Nano Res.* **3** 147
[32] Sahoo S, Gaur A P S, Ahmadi M, Guinel M J F and Katiyar R S 2013 *J. Phys. Chem. C* **117** 9042
[33] Yan R, Simpson J R, Bertolazzi S, Brivio J, Watson M, Wu X, Kis A, Luo T, Hight Walker A R and Xing H G 2014 *ACS Nano* **8** 986
[34] Taube A, Judek J, Lapińska A and Zdrojek M 2015 *ACS Appl. Mater. Interfaces* **7** 5061
[35] Li W, Carrete J and Mingo N 2013 *Appl. Phys. Lett.* **103** 253103
[36] Cai Y, Lan J, Zhang G and Zhang Y W 2014 *Phys. Rev. B* **89** 035438
[37] Jiang J W, Zhuang X Y and Rabczuk T 2013 *Sci. Rep.* **3** 2209
[38] Liu T H, Chen Y C, Pao C W and Chang C C 2014 *Appl. Phys. Lett.* **104** 201909
[39] Wu X, Yang N and Luo T 2015 *Appl. Phys. Lett.* **107** 191907
[40] Zhang J, Hong Y, Wang X, Yue Y, Xie D, Jiang J, Xiong Y and Li P 2017 *J. Phys. Chem. C* **121** 10336
[41] Chen C C, Li Z, Shi L and Cronin S B 2014 *Appl. Phys. Lett.* **104** 081908
[42] Chen J, Walther J H and Koumoutsakos P 2015 *Adv. Funct. Mater.* **25** 7539
[43] Liu X, Zhang G and Zhang Y W 2015 *Nano Res.* **8** 2755
[44] Peng B, Zhang H, Shao H, Xu Y, Zhang X and Zhu H 2016 *RSC Adv.* **6** 5767
[45] Mingo N and Broido D A 2005 *Phys. Rev. Lett.* **95** 096105
[46] Nika D L, Pokatilov E P, Askerrov A S and Balandin A A 2009 *Phys. Rev. B* **79** 155413
[47] Pop E, Varshney V and Roy A K 2012 *MRS Bulletin* **37** 1273
[48] Klemens P G 2000 *J. Wide Bandgap Mater.* **7** 332
[49] Klemens P G 2001 *Int. J. Thermophys.* **22** 265
[50] Jeong C, Datta S and Lundstrom M 2011 *J. Appl. Phys.* **109** 073718
[51] Jo I, Pettes M T, Ou E, Wu W and Shi L 2014 *Appl. Phys. Lett.* **104** 201902
[52] Gu X and Yang R 2014 *Appl. Phys. Lett.* **105** 131903
[53] Zhou W X and Chen K Q 2015 *Sci. Rep.* **5** 15070
[54] Su J, Liu Z T, Feng L P and Li N 2015 *J. Alloys Compd.* **622** 777
[55] Zhang X, Sun D, Li Y, Lee G H, Cui X, Chenet D, You Y, Heinz T F and Hone J C 2015 *ACS Appl. Mater. Interfaces* **7** 25923
[56] Peimyoo N, Shang J, Yang W, Wang Y, Cong C and Yu T 2015 *Nano Res.* **8** 1210
[57] Allain A, Kang J, Banerjee K and Kis A 2015 *Nat. Mater.* **14** 1195
[58] Cui X, Lee G H, Kim Y D, Arefe G, Huang P Y, Lee C H, Chenet D A, Zhang X, Wang L, Ye F, Pizzocchero F, Jessen B S, Watanabe K, Taniguchi T, Muller D A, Low T, Kim P and Hone J 2015 *Nat. Nano* **10** 534
[59] Liu Y, Wu H, Cheng H C, Yang S, Zhu E, He Q, Ding M, Li D, Guo J, Weiss N O, Huang Y and Duan X 2015 *Nano Lett.* **15** 3030
[60] Yu Z, Ong Z Y, Pan Y, Cui Y, Xin R, Shi Y, Wang B, Wu Y, Chen T, Zhang Y W, Zhang G and Wang X 2016 *Adv. Mater.* **28** 547
[61] Liu X, Zhang G and Zhang Y W 2016 *Nano Res.* **9** 2372
[62] Liu X, Zhang G and Zhang Y W 2016 *Nano Lett.* **16** 4954
[63] Liu X, Gao J, Zhang G and Zhang Y W 2017 *Nano Res.* **10** 2944
[64] Ding Z, Pei Q X, Jiang J W, Huang W and Zhang Y W 2016 *Carbon* **96** 888
[65] Judek J, Gertych A P, Swiniarski M, Lapinska A, Duzynska A and Zdrojet M 2015 *Sci. Rep.* **5** 12422
[66] Mao R, Kong B D and Kim K W 2014 *J. Appl. Phys.* **116** 034302
[67] Chen Z, Jang W, Bao W, Lau C N and Dames C 2009 *Appl. Phys. Lett.* **95** 161910
[68] Liu Y, Ong Z Y, Wu J, Zhao Y, Watanabe K, Taniguchi T, Chi D, Zhang G, Thong J T L, Qiu C W and Hippalgaonkar K 2017 *Sci. Rep.* **7** 43886
[69] Yuan P, Li C, Xu S, Liu J and Wang X 2017 *Acta Materialia* **122** 152
[70] Liu W, Kang J, Cao W, Sarkar D, Khatami Y, Jena D and Banerjee K 2013 *IEEE International Electron Devices Meeting* **499** 19.4.1–19.4.4
[71] Kang J, Liu W, Sarkar D, Jena D and Banerjee K 2014 *Phys. Rev. X* **4** 031005
[72] Hu L, Desai T and Keblinski P 2011 *Phys. Rev. B* **83** 195423
[73] Liu X, Zhang G and Zhang Y W 2015 *Carbon* **94** 760
[74] Liu X, Gao J, Zhang G and Zhang Y W 2017 *Adv. Funct. Mater.* **27** 1702776
[75] Liu X, Zhang G and Zhang Y W 2014 *J. Phys. Chem. C* **118** 12541
[76] Balandin A A, Ghosh S, Bao W, Calizo I, Teweldebrhan D, Miao F and Lau C N 2008 *Nano Lett.* **8** 902
[77] Ghosh S, Bao W, Nika D L, Subrina S, Pokatilov E P and Ning C 2010 *Nat. Mater.* **9** 555
[78] Seol J H, Jo I, Moore A L, Lindsay L, Aitken Z H, Pettes M T, Li X, Yao Z, Huang R, Broido D, Mingo N, Ruoff R S and Shi L 2010 *Science* **328** 213
[79] Sadeghi M M, Jo I and Shi L 2013 *Proceedings of the National Academy of Sciences of the United States of America* **110** 16321
[80] Schelling P K, Phillpot S R and Keblinski P 2002 *Appl. Phys. Lett.* **80** 2484
[81] Xu W, Zhang G and Li B 2014 *J. App. Phys.* **116** 134303
[82] Sutter P, Cortes R, Lahiri J and Sutter E 2012 *Nano Lett.* **12** 4869
[83] Liu L, Park J, Siegel D A, McCarty K F, Clark K W, Deng W, Basile L, Idrobo J C, Li A P and Gu G 2014 *Science* **343** 163